Accurate X-Ray Spectral Predictions: An Advanced Self-Consistent-Field Approach Inspired by Many-Body Perturbation Theory

Yufeng Liang,[1] John Vinson,[2] Sri Pemmaraju,[1] Walter S. Drisdell,[3] Eric L. Shirley,[2] and David Prendergast[1]
[1]*The Molecular Foundry, Lawrence Berkeley National Laboratory, Berkeley, California 94720, USA*
[2]*National Institute of Standards and Technology (NIST), Gaithersburg, Maryland 20899, USA*
[3]*Chemical Sciences Division, Lawrence Berkeley National Laboratory, Berkeley, California 94720, USA*
(Received 1 September 2016; revised manuscript received 27 January 2017; published 3 March 2017)

Constrained-occupancy delta-self-consistent-field (ΔSCF) methods and many-body perturbation theories (MBPT) are two strategies for obtaining electronic excitations from first principles. Using the two distinct approaches, we study the O 1*s* core excitations that have become increasingly important for characterizing transition-metal oxides and understanding strong electronic correlation. The ΔSCF approach, in its current single-particle form, systematically underestimates the pre-edge intensity for chosen oxides, despite its success in weakly correlated systems. By contrast, the Bethe-Salpeter equation within MBPT predicts much better line shapes. This motivates one to reexamine the many-electron dynamics of x-ray excitations. We find that the single-particle ΔSCF approach can be rectified by explicitly calculating many-electron transition amplitudes, producing x-ray spectra in excellent agreement with experiments. This study paves the way to accurately predict x-ray near-edge spectral fingerprints for physics and materials science beyond the Bethe-Salpether equation.

DOI: 10.1103/PhysRevLett.118.096402

X-ray absorption spectroscopy (XAS) is a powerful characterization technique in physics, chemistry, and materials science, owing to its element specificity and orbital selectivity. With the help of density-functional theory (DFT), the interpretation of XAS is greatly facilitated by simulating spectral fingerprints for hypothetical structures from first principles. Satisfactory x-ray absorption spectra have been simulated across a wide range of systems from small molecules [1,2] to condensed matter [3–9] and even complex interfaces [10].

In this Letter, we introduce a novel first principles theory for simulating x-ray absorption spectra, extending the constrained-occupancy delta-self-consistent-field (ΔSCF) method [6,7,9]. The ΔSCF method assumes a fixed core-hole potential and employs only single-particle orbitals for finding transition amplitudes. It is generally thought that this theory cannot capture certain many-electron effects as incorporated in many-body perturbation theories, such as the Bethe-Salpeter Equation (BSE) [11–14]. However, if the one-body transition amplitude in the ΔSCF method is recast into a many-body formalism, we show that the method can in fact, capture many-electron effects in x-ray excitations. Furthermore, we outline how the excitation spectrum can be enriched by considering multiple electron-hole (*e*-*h*) excitations, permitting extensions beyond the BSE, on the level of the Mahan–Noziéres–De Dominicis (MND) theory [15,16].

For our examples, we choose the O *K* edges ($1s \rightarrow np$ transitions) of transition-metal oxides (TMOs) to illustrate the utility of the many-body ΔSCF method. The study of the O *K* edges for TMOs is fueled by the quest for next-generation energy materials, for rechargeable battery cathodes [17–20], fuel cells [21,22], water-splitting catalysts [23–25], and transparent conductive layers [26]. Many of these materials are TMOs with complex chemical properties due to their *d* orbitals. Additionally, XAS has been employed to understand electron correlations inherent in TMOs, such as metal-insulator transitions [27–29], high-T_c superconductivity [30,31], and emergent phenomena at perovskite interfaces [32]. XAS can also serve as a powerful guide to advance theories for correlated electron systems, including the DFT + U method [33], dynamical mean-field theory [34], and exact diagonalization approaches [35,36]. In almost all of the aforementioned examples [17,19–21,23–28,30–33,35,36], there are measurements at the O *K* edge. Despite its utility, very few studies have simulated this absorption edge for TMOs from first principles.

Five TMOs are selected for benchmarking: the rutile TiO_2, VO_2, and CrO_2, as well as the corundum α-Fe_2O_3 and the perovskite $SrTiO_3$. They vary greatly in structure, band gap, or magnetism. The rutile VO_2 (> 340 K) and CrO_2 are metallic, whereas TiO_2 and $SrTiO_3$ are insulating. CrO_2 is ferromagnetic (FM), while Fe_2O_3 is antiferromagnetic (AFM). The O *K* edges from previous experiments [23,27,37–39] are shown in Fig. 1(a). These spectra are angularly averaged except for CrO_2, where the polarization is perpendicular to the magnetization axis [38]. The TM-3*d*-O-2*p* hybridization manifests as sharp double peaks around 530 eV, which result from the t_{2g}-e_g splitting in the octahedral field. The intensity ratio of the two peaks often serves as a diagnostic tool. Understanding gained

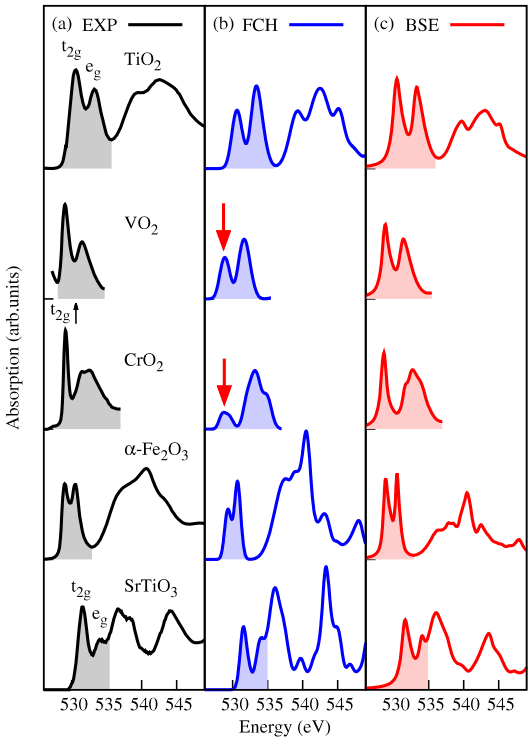

FIG. 1. A comparison of experimental O K edges (a) with the simulated spectra by the FCH approach (b) and BSE (c). The pre-edge regions are covered by shaded areas. Spectra are normalized according to the e_g peak intensity. The severely underestimated t_{2g} peaks are marked by red arrows.

through these simple transition metal (TM) compounds will find great utility in interpreting XAS for more complex contexts, e.g., liquids, interfaces, heterogenous materials, where other characterization techniques such as x-ray diffraction are less effective. For instance, the O K-edge peak intensities have been used to deduce oxygen redox chemistry in rechargeable battery cathodes [20], and yet, the correlation between experimental spectra and first principles modeling of structures remains to be established in the absence of accurate predictions of the near-edge line shape.

The x-ray absorbance $\sigma(\omega)$ is obtained from Fermi's golden rule

$$\sigma(\omega) \propto \omega \sum_f |\langle \Psi_f | \boldsymbol{\epsilon} \cdot \boldsymbol{R} | \Psi_i \rangle|^2 \delta(E_f - E_i - \hbar\omega), \quad (1)$$

where $\boldsymbol{\epsilon}$ and $\boldsymbol{R}$ are the photon polarization and many-body position operator, respectively. $|\Psi_i\rangle$ is the initial (ground) state and $|\Psi_f\rangle$ is any excited eigenstate of the system, while E_i and E_f are their energies. Predicting x-ray absorption requires: (a) an accurate prediction of the excitation energies E_f and (b) a reliable approximation of the amplitude $\langle \Psi_f | \boldsymbol{\epsilon} \cdot \boldsymbol{R} | \Psi_i \rangle$. We first contrast the single-particle ΔSCF core-hole approach and the BSE using the five TMOs and identify a systematic failure in the current ΔSCF method. We argue that the failure is due to the omission of many-electron response to the core hole, which motivates us to develop an advanced ΔSCF approach by using many-electron wave functions instead of single-particle orbitals.

ΔSCF *and BSE Approaches*.—In the ΔSCF core-hole approach, the core-excited atom is treated as a single impurity with one electron removed from the excited core level. Depending on whether or not the x-ray photoelectron is included, it is termed as an excited-electron and core-hole (XCH) or full core-hole (FCH) calculation [6,7,9]. One places the core-excited atom in a sufficiently large supercell and then finds the equilibrated electron density using constrained-occupancy DFT. This equilibrated state, with the presence of a core hole, is referred to as the *final state* [13] and that of the pristine system as the *initial state*. The working approximation is to use single Kohn-Sham orbitals for finding the transition amplitude

$$\langle \Psi_f | \boldsymbol{\epsilon} \cdot \boldsymbol{R} | \Psi_i \rangle \approx S \langle \tilde{\psi}_f | \boldsymbol{\epsilon} \cdot \boldsymbol{r} | \psi_h \rangle, \quad (2)$$

where $\tilde{\psi}_f$'s are the unoccupied orbitals in the final state (with tilde), and ψ_h is the core orbital in the initial state. S is a many-body overlap that reflects the excited-state response of the remaining electrons other than the photoexcited one and is normally treated as a constant in the sudden approximation [40]. The excitation spectrum $E_f - E_i$ is approximated based on differences in DFT orbital energies, $\tilde{\varepsilon}_f - \varepsilon_h$, with some further realignment reflecting the local atomic context and the experimental energy scale [41].

To account for strong electron correlations in TMOs, the DFT + U theory [33] is employed where the DFT energy is captured by the Perdew-Burke-Ernzerhof (PBE) functional, and the on-site Coulomb potential U are from Ref. [42]. We interpret the DFT + U orbital energies as quasiparticle (QP) energies and perform FCH rather than XCH calculations so as not to favor any particular occupation. More numerical details can be found in the Supplemental Material [43]. Strikingly, the FCH approach systematically underestimates the intensity of the near-edge peak associated with the t_{2g} manifold for all selected TMOs [Fig. 1(b)]. The t_{2g} peak at ~529.2 eV of CrO_2 [38] suffers from the most severe underestimation. It becomes a weak, broad feature in the FCH simulation as compared to the strong, sharp peak in experiment. The t_{2g}-e_g peak intensity ratios of VO_2 and Fe_2O_3 are also too low—both are predicted as 0.7, compared with 1.7 and 1.0 as measured, respectively.

In the BSE formalism [12,46,47], the final state is assumed to be a superposition of effective e-h pairs and the matrix elements are calculated as

$$\langle \Psi_f | \boldsymbol{\epsilon} \cdot \boldsymbol{R} | \Psi_i \rangle = \sum_c A_c^{f*} \langle \psi_c | \boldsymbol{\epsilon} \cdot \boldsymbol{r} | \psi_h \rangle, \quad (3)$$

where ψ_c's are the *initial-state* orbitals and c iterates over *empty* orbitals only. The exciton amplitude A_c^f and energy

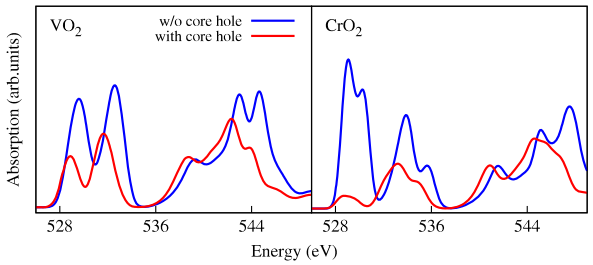

FIG. 2. A comparison of the spectra with and without (w/o) the core hole in the ΔSCF calculations.

E_f can be solved from the BSE as in Ref. [11–14]. The core-level BSE calculations in this work employ the OCEAN code [14,48].

As is shown in Fig. 1(c), the BSE substantially improves on the O K-edge line shapes. The "t_{2g}" peak intensity is retrieved for each investigated TMO, particularly for CrO_2. The simulated t_{2g}-e_g intensity ratios are almost as measured for TiO_2, α-Fe_2O_3, and $SrTiO_3$ (below 537 eV). These BSE spectra are also in better agreement with experiments than the previous results using the initial-state rule [49,50].

In fact, the core-hole effects predicted by the ΔSCF method in these oxides are counterintuitive. Typically, excitonic effects tend to sharpen the absorption edge due to e-h attraction [5,11,12,46]. In Fig. 2, we show the core-hole effects from ΔSCF by comparing the initial- and final-state spectra. The core-hole attraction does redshift the spectra by over 1 eV in both the TM $3d$ pre-edge and the $4sp$ [51] region (near 544 eV). However, the FCH core-hole effect substantially reduces the t_{2g} peak intensity. Similarly underestimated prepeak intensity was encountered before [52–54], but no satisfactory explanation has been provided to date.

With this comparison, we can now explain why the one-body ΔSCF formalism tends to underestimate the peak intensity. The single-particle approximation in Eq. (2), $S\langle\tilde{\psi}_f|\boldsymbol{\epsilon}\cdot\boldsymbol{r}|\psi_h\rangle$, does not contain any information about the initial state of the valence electrons when S is a constant. The spectrum is found by summing up single-particle transitions in the final state in which the valence electrons have already equilibrated with the core hole. The final-state picture alone does not reflect the full process of x-ray excitations: first a core hole is generated by an x-ray photon, then the valence electrons begin to relax in presence of the core-hole potential. This is why the final-state spectra predicted by the one-body formalism can be subject to spurious charge transfer effects if the electron density happens to transfer onto the optically active orbitals due to core-hole attraction. In the above examples of O $1s$ excitations, a substantial amount of electron density is transferred into the $2p$ character local to the excited O (0.55 e^- for TiO_2 and 0.72 e^- for CrO_2), which blocks some bright transitions from $1s \rightarrow 2p$ and leads to the reduced pre-edge intensity. Conversely, a many-body perturbation theory, such as the BSE, considers the evolution of many-electron systems using diagrammatic approaches, which are capable of capturing the correct time ordering and dynamics in photoexcitations. This can be seen in Eq. (3); the BSE begins with empty initial-state orbitals and considers their hybridization under the core-hole effect, hence retrieving the edge sharpness.

Many-Electron Formalism.—To alleviate the deficiencies of the one-body ΔSCF method, we seek a better approximation to $\langle\Psi_f|\boldsymbol{\epsilon}\cdot\boldsymbol{R}|\Psi_i\rangle$ so as to incorporate the many-electron response as the system evolves from the initial to final state. We abandon the single-particle approximation used in Eq. (2) and develop an approximate many-electron wave function. To avoid solving an intractable full configuration-interaction problem and leverage the current ΔSCF approach, we assume that the valence Kohn-Sham (KS) orbitals are *noninteracting*. Consequently, a single Slater determinant comprising the KS orbitals is a consistent many-electron eigenstate. This approximation is analogous to the independent-electron model with a single core-hole considered in the MND theory [15,16]. It may fail to capture certain many-body correlations and we will defer this discussion until later.

Within the independent-KS-orbital approximation, the ground state $|\Psi_i\rangle$ can be constructed as a Slater determinant built from the N lowest occupied valence orbitals of the pristine supercell and the core orbital of the impurity atom. Here, N is the number of valence electrons in the supercell. Similarly, the final state $|\Psi_f\rangle$ can be constructed as a Slater determinant of arbitrary $N+1$ KS orbitals in the final-state picture. To enumerate the many-electron final states, we generalize the final-state index f to represent any excited configuration of these $N+1$ electrons: f now represents a unique $(N+1)$-tuple, $f = (f_1, f_2, \ldots, f_{N+1})$, where f_i's label distinct final-state orbitals that the $N+1$ electrons can occupy.

The single-particle orbitals necessary for constructing $|\Psi_i\rangle$ and $|\Psi_f\rangle$ can be readily obtained from respective ΔSCF calculations performed over the supercell. However, $|\Psi_i\rangle$ and $|\Psi_f\rangle$ are represented with the initial- and final-state orbital bases, respectively. To eventually access $\langle\Psi_f|\boldsymbol{\epsilon}\cdot\boldsymbol{R}|\Psi_i\rangle$, we perform the orbital transformation from the initial to final state: $|\tilde{\psi}_i\rangle = \sum_j|\psi_j\rangle\langle\psi_j|\tilde{\psi}_i\rangle = \sum_j\xi_{ij}|\psi_j\rangle$, in which $\tilde{\psi}_i$ and ψ_j are the i^{th} final-state and j^{th} initial-state orbitals in the supercell, respectively. ξ_{ij} is the transformation coefficient. The resulting matrix element has the same form as in Eq. (3), but the amplitude of a given final state f becomes a single determinant of the transformation coefficients [43]

$$A_c^f = \det\begin{bmatrix} \xi_{f_1,1} & \xi_{f_1,2} & \cdots & \xi_{f_1,N} & \xi_{f_1,c} \\ \xi_{f_2,1} & \xi_{f_2,2} & \cdots & \xi_{f_2,N} & \xi_{f_2,c} \\ \vdots & & \vdots & & \vdots \\ \xi_{f_{N+1},1} & \xi_{f_{N+1},2} & \cdots & \xi_{f_{N+1},N} & \xi_{f_{N+1},c} \end{bmatrix}. \quad (4)$$

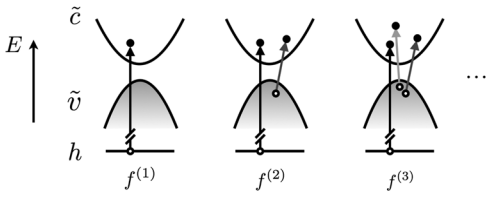

FIG. 3. Schematic of the excitation configurations in the *final-state* space. h indicates the single core level, while $\tilde{c}$ and $\tilde{v}$ indicate the empty and occupied orbtial spaces, respectively.

Within the independent-KS-orbital approximation, the energy of $|\Psi_f\rangle$ can be found by summing up the energies of the occupied KS orbitals in the *final state*

$$E_f = \sum_{j=1}^{N+1} \tilde{\varepsilon}_{f_j}. \tag{5}$$

The energy difference $E_f - E_i$ for producing spectra may employ a similar alignment scheme as in the single-body approach, since the initial- (ground-) state energy E_i is fixed. In the following discussion, it is more meaningful to define the relative energy $\Omega_f = E_f - E_{\text{th}}$, where the threshold energy, $E_{\text{th}} = \sum_{j=1}^{N+1} \tilde{\varepsilon}_j$, corresponds to the lowest-energy final-state configuration $(1, 2, \ldots, N+1)$.

Determinant expressions similar to Eq. (4) were also obtained in previous work [55–57], but they are rarely applied in a solid-state context from first principles. Thus, it is of great interest to examine whether the many-electron ΔSCF formalism in Eq. (4) and (5) can reproduce the correct line shapes for the investigated TMOs.

Evaluating the many-electron A_c^f seems formidable at first glance because a solid contains many electrons, which leads to a combinatorially huge number of final states. To facilitate the calculation, we regroup the final-state configurations according to the number of *e-h* pairs excited. For example, we denote a *single* configuration with one core-excited *e-h* pair as $f^{(1)} = (1, 2, \ldots, N, f_{N+1})$, which is used in producing the one-body ΔSCF XAS, and f_{N+1} is the single unoccupied orbital in the final state. Based on this configuration, we can define a *double* configuration with one more valence *e-h* pairs as $f^{(2)} = (1, \ldots, i-1, i+1, \ldots, N, f_N, f_{N+1})$, where $f_{N+1} > f_N > N$ and so forth (Fig. 3).

Despite a large number of excitation configurations, not all of them contribute equally to the near-edge XAS, particularly near the absorption onset. First, for an insulator, Ω_f will increase proportionally with the number n of *e-h* pairs excited across the band gap (E_g): $\Omega_f \geq (n-1)E_g$. This significantly reduces the number of necessary final states for producing the first few eVs of XAS for an insulator. Second, the many-electron transition amplitude may decrease rapidly with an increasing number of *e-h* pairs excited as we will show next.

We reexamine two extreme cases: the insulating TiO_2 and the metallic CrO_2. Figure 4 shows the XAS calculated

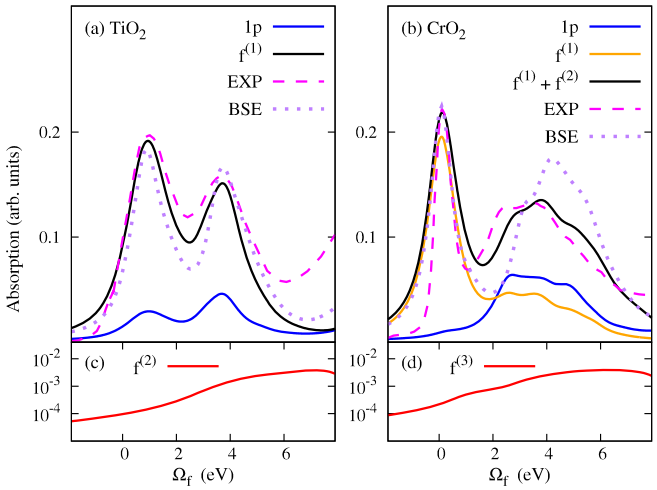

FIG. 4. ΔSCF XAS rectified by the many-electron matrix formalism for TiO_2 (a) and CrO_2 (b). For comparison, the spectra produced by the one-body FCH formalism are denoted as 1p, and experimental (EXP) and BSE spectra as in Fig. 1 are also added with the first peaks aligned. (c) and (d) show the higher-order intensity contributions (in log scale) that do not exceed 0.004 in both cases.

from the many-body formalism as in Eqs. (4) and (5). The orbitals used for calculating the transformation coefficients ξ_{ij} in A_c^f are obtained from the same set of ground state and FCH calculations [43] as previously described. For simplicity, only the states at the Γ point of the supercell Brillouin zone are used for producing the XAS. Remarkably, the simulated XAS line shapes (Fig. 4), with the many-electron formalism, are in excellent agreement with experiments. In particular, for CrO_2, the edge sharpness is completely retrieved [Fig. 4(b)], despite the disappearance of the first peak in a single-electron theory.

We find calculated XAS for TiO_2 converges at the order of $f^{(1)}$. As expected, the contributions from $f^{(2)}$ (Fig. 4(c)] appear at higher energies due to the sizable band gap and are much weaker due to reduced wave function overlap. However, it is more challenging to achieve numerical convergence in the metallic CrO_2. While the first peak is retrieved mainly from $f^{(1)}$ excitations, the correct peak-intensity ratio can only be reproduced when the next-order, $f^{(2)}$, is taken into account, which substantially increases the intensity of the absorption feature ~4 eV above onset [Fig. 4(b)]. Meanwhile, we find $f^{(3)}$ can be neglected up to the first 8 eV [Fig. 4(d)].

Both the BSE (Fig. 1) and the many-electron formalism (Fig. 4) yield very similar spectra for TiO_2, but the many-electron formalism produces a spectrum for CrO_2 in closer agreement with experiment than the BSE. The peak-intensity ratio is 1.7 from the experiment, 1.6 from the many-electron formalism, but only 1.3 from the BSE. We attribute this improvement to the explicit inclusion of many-electron response to the core-hole potential via the

transition amplitude A_c^f [Eq. (4)]. Since the Slater determinants are exact solutions to the independent-electron model, the many-electron formalism has taken into account all possible many-electron processes in the MND theory. In addition to the *e-h* ladder diagrams in the BSE, the MND theory also considers nonladder diagrams, such as diagrams with crossing Coulomb lines and bubble diagrams that account for the orthogonality catastrophe [15,16,55]. Instead of adopting a diagrammatic approach, the many-electron formalism considers these processes via incorporating the response of each electron to the core hole in the determinant amplitude A_c^f. Therefore, the many-electron formalism goes beyond the two-particle correlation in the BSE. For insulators like TiO_2, the many-electron formalism produces results very similar to the BSE because the nonladder diagrams are not important near the absorption edge. However, this is not the case for CrO_2 since multiple *e-h*-pair production is more likely in a metal, and the nonladder diagrams become significant for determining the near-edge line shape. The significance of the multiple electron response can also be appreciated from the fact that the CrO_2 spectrum converges at a higher order $f^{(n)}$.

At last, we briefly discuss the validity of the independent-KS-orbital approximation. On the $f^{(1)}$ level, there is a one-to-one correspondence between the many-electron configurations and the empty single-particle final-state orbitals, and the latter are typically good approximations of QP band topology and wave functions [46,58]. This approximation may break down if there are one or more valence *e-h* pairs. For example, valence *e-h* pairs in the $f^{(2)}$ configurations of an insulator may hybridize to form bound excitons; the two excited electrons in the $f^{(2)}$ configurations may interact through strong on-site Coulomb repulsion. In the case of CrO_2, however, the strong metallic screening can largely reduce *e-h* binding energy, maintaining the independent-KS-orbital approximation. As for strongly correlated effects, it will be worthwhile to further consider embedded models based on the current determinant formalism.

Conclusions.—We have shown that the BSE and a newly developed many-electron ΔSCF approach are highly predictive for O *K*-edge fingerprints of TMOs. The systematic underestimation of the peak-intensity ratio within the original one-body ΔSCF approach is attributed to the absence of many-electron response in this formalism. We have demonstrated how to rectify these shortcomings by (1) extending the wave functions in the original ΔSCF to a many-electron form and (2) calculating the determinant form of the transition amplitude. This many-electron formalism is transferable and not at all peculiar to TMOs. We leave the discussion of shakeup effects, improvement of efficiency, and other examples to near-future work.

Theoretical and computational work was performed by Y. L. and D. P. at The Molecular Foundry, which is supported by the Office of Science, Office of Basic Energy Sciences, of the United States Department of Energy under Contact No. DE-AC02-05CH11231. W. S. D. was supported by the Joint Center for Artificial Photosynthesis, a DOE Energy Innovation Hub, supported through the Office of Science of the U.S. Department of Energy (Award No. DE-SC0004993). We acknowledge fruitful discussion with Chunjing Jia (Y. L.) and Bill Gadzuk (J. V.). We also would like to acknowledge the referees for giving very patient, professional, and thoughtful comments in the review process. Computations were performed with the computing resources at the National Energy Research Scientific Computing Center (NERSC).

[1] J. S Uejio, C. P Schwartz, R. J Saykally, and D. Prendergast, Effects of vibrational motion on core-level spectra of prototype organic molecules, Chem. Phys. Lett. **467**, 195 (2008).

[2] L. Triguero, L. G. M. Pettersson, and H. Ågren, Calculations of near-edge x-ray-absorption spectra of gas-phase and chemisorbed molecules by means of density-functional and transition-potential theory, Phys. Rev. B **58**, 8097 (1998).

[3] T. Mizoguchi, I. Tanaka, M. Yoshiya, F. Oba, K. Ogasawara, and H. Adachi, Core-hole effects on theoretical electron-energy-loss near-edge structure and near-edge x-ray absorption fine structure of MgO, Phys. Rev. B **61**, 2180 (2000).

[4] S.-D. Mo and W. Y. Ching, *Ab initio* calculation of the core-hole effect in the electron energy-loss near-edge structure, Phys. Rev. B **62**, 7901 (2000).

[5] G. Duscher, R. Buczko, S. J. Pennycook, and S. T. Pantelides, Core-hole effects on energy-loss near-edge structure, Ultramicroscopy **86**, 355 (2001).

[6] M. Taillefumier, D. Cabaret, A.-M. Flank, and F. Mauri, X-ray absorption near-edge structure calculations with the pseudopotentials: Application to the K edge in diamond and α-quartz, Phys. Rev. B **66**, 195107 (2002).

[7] B. Hetényi, F. De Angelis, P. Giannozzi, and R. Car, Calculation of near-edge x-ray-absorption fine structure at finite temperatures: Spectral signatures of hydrogen bond breaking in liquid water., J. Chem. Phys. **120**, 8632 (2004).

[8] M. Cavalleri, M. Odelius, D. Nordlund, A. Nilsson, and L. G. Pettersson, Half or full core hole in density functional theory x-ray absorption spectrum calculations of water?, Phys. Chem. Chem. Phys. **7**, 2854 (2005).

[9] D. Prendergast and G. Galli, X-Ray Absorption Spectra of Water from First Principles Calculations, Phys. Rev. Lett. **96**, 215502 (2006).

[10] J.-J. Velasco-Velez, C. H. Wu, T. . Pascal, L. F. Wan, J. Guo, D. Prendergast, and M. Salmeron, The structure of interfacial water on gold electrodes studied by x-ray absorption spectroscopy, Science **346**, 831 (2014).

[11] E. L. Shirley, Ab Initio Inclusion of Electron-Hole Attraction: Application to X-Ray Absorption and Resonant Inelastic X-Ray Scattering, Phys. Rev. Lett. **80**, 794 (1998).

[12] L. X. Benedict, E. L. Shirley, and R. B. Bohn, Optical Absorption of Insulators and the Electron-Hole Interaction: An *Ab Initio* Calculation, Phys. Rev. Lett. **80**, 4514 (1998).

[13] J. J. Rehr, J. A. Soininen, and E. L. Shirley, Final-state rule vs the bethe-salpeter equation for deep-core x-ray absorption spectra, Phys. Scr. **2005**, 207 (2005).
[14] J. Vinson, J. J. Rehr, J. J. Kas, and E. L. Shirley, Bethe-salpeter equation calculations of core excitation spectra, Phys. Rev. B **83**, 115106 (2011).
[15] Ph. Nozieres and C. T. De Dominicis, Singularities in the x-ray absorption and emission of metals. iii. one-body theory exact solution, Phys. Rev. **178**, 1097 (1969).
[16] G. D. Mahan, *Many-Particle Physics* (Springer Science & Business Media, Chicago, 2013).
[17] N. Yabuuchi, K. Yoshii, S.-T. Myung, I. Nakai, and S. Komaba, Detailed studies of a high-capacity electrode material for rechargeable batteries, Li_2MnO_3-$LiCo_{1/3}Ni_{1/3}Mn_{1/3}O_2$, J. Am. Chem. Soc. **133**. 4404 (2011).
[18] Y.-Y. Hu, Z. Liu, K.-W. Nam, O. J. Borkiewicz, J. Cheng, X. Hua, M. T. Dunstan, X. Yu, K. M. Wiaderek, L.-S. Du *et al.*, Origin of additional capacities in metal oxide lithium-ion battery electrodes, Nat. Mater. **12**, 1130 (2013).
[19] F. Lin, D. Nordlund, Y. Li, M. K. Quan, L. Cheng, T.-C. Weng, Y. Liu, H. L. Xin, and M. M. Doef, Metal segregation in hierarchically structured cathode materials for high-energy lithium batteries, Nat. Energy **1**, 15004 (2016).
[20] K. Luo, M. R. Roberts, R. Hao, N. Guerrini, D. M. Pickup, Y.-S. Liu, K. Edström, J. Guo, A. V. Chadwick, L. C. Duda *et al.*, Charge-compensation in 3d-transition-metal-oxide intercalation cathodes through the generation of localized electron holes on oxygen, Nat. Chem. **8**, 684 (2016).
[21] J. Suntivich, H. A. Gasteiger, N. Yabuuchi, H. Nakanishi, J. B. Goodenough, and Y. Shao-Horn, Design principles for oxygen-reduction activity on perovskite oxide catalysts for fuel cells and metal–air batteries, Nat. Chem. **3**, 546 (2011).
[22] P. Strasser, S. Koh, T. Anniyev, J. Greeley, K. More, C. Yu, Z. Liu, S. Kaya, D. Nordlund, H. Ogasawara *et al.*, Lattice-strain control of the activity in dealloyed core–shell fuel cell catalysts, Nat. Chem. **2**, 454 (2010).
[23] G.-z. Zhu, G. Radtke, and G. A. Botton, Bonding and structure of a reconstructed (001) surface of $SrTiO_3$ from tem, Nature (London) **490**, 384 (2012).
[24] M. Matsukawa, R. Ishikawa, T. Hisatomi, Y. Moriya, N. Shibata, J. Kubota, Y. Ikuhara, and K. Domen, Enhancing photocatalytic activity of $LaTiO_2N$ by removal of surface reconstruction layer, Nano Lett. **14**, 1038 (2014).
[25] A. Grimaud, K. J. May, C. E. Carlton, Y.-L. Lee, M. Risch, W. T. Hong, J. Zhou, and Y. Shao-Horn, Double perovskites as a family of highly active catalysts for oxygen evolution in alkaline solution, Nat. Commun. **4** 2439 (2013).
[26] Z. Lebens-Higgins, D. O. Scanlon, H. Paik, S. Sallis, Y. Nie, M. Uchida, N. F. Quackenbush, M. J. Wahila, G. E. Sterbinsky, Dario A. Arena *et al.*, Direct Observation of Electrostatically Driven Band Gap Renormalization in a Degenerate Perovskite Transparent Conducting Oxide, Phys. Rev. Lett. **116**, 027602 (2016).
[27] T. C. Koethe, Z. Hu, M. W. Haverkort, C. Schüßler-Langeheine, F. Venturini, N. B. Brookes, O. Tjernberg, W. Reichelt, H. H. Hsieh, H.-J Lin *et al.*, Transfer of Spectral Weight and Symmetry Across the Metal-Insulator Transition in VO_2, Phys. Rev. Lett. **97**, 116402 (2006).
[28] D. Ruzmetov, S. D. Senanayake, and S. Ramanathan, X-ray absorption spectroscopy of vanadium dioxide thin films across the phase-transition boundary, Phys. Rev. B **75**, 195102 (2007).
[29] N. B. Aetukuri, A. X. Gray, M. Drouard, M. Cossale, L. Gao, A. H. Reid, R. Kukreja, H. Ohldag, C. A. Jenkins, E. Arenholz *et al.*, Control of the metal-insulator transition in vanadium dioxide by modifying orbital occupancy, Nat. Phys. **9**, 661 (2013).
[30] C. T. Chen, F. Sette, Y. Ma, M. S. Hybertsen, E. B. Stechel, W. M. C. Foulkes, M. Schulter, S. W. Cheong, A. S. Cooper, L. W. Rupp, Jr *et al.*, Electronic States in $La_{2-x}Sr_xCuO_{4+\delta}$ Probed by Soft-X-Ray Absorption, Phys. Rev. Lett. **66**, 104 (1991).
[31] D. C. Peets, D. G. Hawthorn, K. M. Shen, Y.-J. Kim, D. S. Ellis, H. Zhang, S. Komiya, Y. Ando, G. A. Sawatzky, R. Liang *et al.*, X-Ray Absorption Spectra Reveal the Inapplicability of the Single-Band Hubbard Model to Overdoped Cuprate Superconductors, Phys. Rev. Lett. **103**, 087402 (2009).
[32] J.-S. Lee, Y. W. Xie, H. K. Sato, C. Bell, Y. Hikita, H. Y. Hwang, and C.-C. Kao, Titanium dxy ferromagnetism at the $LaALO_3/SrTIO_3$ interface, Nat. Mater. **12**, 703 (2013).
[33] S. L. Dudarev, G. A. Botton, S. Y. Savrasov, C. J. Humphreys, and A. P. Sutton, Electron-energy-loss spectra and the structural stability of nickel oxide: An LSDA + U study, Phys. Rev. B **57**, 1505 (1998).
[34] V. I. Anisimov, Dm. M. Korotin, M. A. Korotin, A. V. Kozhevnikov, J. Kuneś, A. O. Shorikov, S. L. Skornyakov, and S. V. Streltsov, Coulomb repulsion and correlation strength in lafeaso from density functional and dynamical mean-field theories, J. Phys. Condens. Matter **21**, 075602 (2009).
[35] X. Wang, Luca de' Medici, and A. J. Millis, Theory of oxygen K edge x-ray absorption spectra of cuprates, Phys. Rev. B **81**, 094522 (2010).
[36] C.-C. Chen, M. Sentef, Y. F. Kung, C. J. Jia, R. Thomale, B. Moritz, A. P. Kampf, and T. P. Devereaux, Doping evolution of the oxygen k-edge x-ray absorption spectra of cuprate superconductors using a three-orbital Hubbard model, Phys. Rev. B **87**, 165144 (2013).
[37] W. Yan, Z. Sun, Z. Pan, Q. Liu, T. Yao, Z. Wu, C. Song, F. Zeng, Y. Xie, T. Hu *et al.*, Oxygen vacancy effect on room-temperature ferromagnetism of rutile Co: TiO_2 thin films, Appl. Phys. Lett. **94**, 042508 (2009).
[38] C. B. Stagarescu, X. Su, D. E. Eastman, K. N. Altmann, F. J. Himpsel, and A. Gupta, Orbital character of o- 2p unoccupied states near the fermi level in CrO_2, Phys. Rev. B **61**, R9233 (2000).
[39] S. Shen, J. Zhou, C.-L. Dong, Y. Hu, E. N. Tseng, P. Guo, L. Guo, and S. S. Mao, Surface engineered doping of hematite nanorod arrays for improved photoelectrochemical water splitting, Sci. Rep. **4**, 6627 (2014).
[40] J. J. Rehr, J. Mustre de Leon, S. I. Zabinsky, and R. C. Albers, Theoretical x-ray absorption fine structure standards, J. Am. Chem. Soc. **113**, 5135 (1991).
[41] P. Jiang, D. Prendergast, F. Borondics, S. Porsgaard, L. Giovanetti, E. Pach, J. Newberg, H. Bluhm, F. Besenbacher, and M. Salmeron, Experimental and theoretical investigation of the electronic structure of Cu_2O and CuO thin films on

cu(110) using x-ray photoelectron and absorption spectroscopy, J. Chem. Phys. **138**, 024704 (2013).
[42] L. Wang, T. Maxisch, and G. Ceder, Oxidation energies of transition metal oxides within the GGA + U framework, Phys. Rev. B **73**, 195107 (2006).
[43] See Supplemental Material at http://link.aps.org/supplemental/10.1103/PhysRevLett.118.096402 for computational details, parameter settings, and the derivation of the many-electron amplitude A^{f_c}, which includes Ref. [44,45].
[44] P. Giannozzi *et al.*, Quantum espresso: a modular and open-source software project for quantum simulations of materials, J. Phys. Condens. Matter **21**, 395502 (2009).
[45] E. L. Shirley, Optimal basis sets for detailed brillouin-zone integrations, Phys. Rev. B **54**, 16464 (1996).
[46] M. Rohlfing and S. G. Louie, Electron-hole excitations and optical spectra from first principles, Phys. Rev. B **62**, 4927 (2000).
[47] G. Onida, L. Reining, and A. Rubio, Electronic excitations: density-functional versus many-body green?s-function approaches, Rev. Mod. Phys. **74**, 601 (2002).
[48] K. Gilmore, J. Vinson, E. L. Shirley, D. Prendergast, C. D. Pemmaraju, J. J. Kas, F. D. Vila, and J. J Rehr, Efficient implementation of core-excitation bethe–salpeter equation calculations, Comput. Phys. Commun. **197**, 109 (2015).
[49] F. De Groot and A. Kotani, *Core Level Spectroscopy of Solids* (CRC Press, New York, 2008).
[50] F. De Groot, High-resolution x-ray emission and x-ray absorption spectroscopy, Chem. Rev. **101**, 1779 (2001).
[51] F. M. F. De Groot, M. Grioni, J. C. Fuggle, J. Ghijsen, G. A. Sawatzky, and H. Petersen, Oxygen 1s x-ray-absorption edges of transition-metal oxides, Phys. Rev. B **40**, 5715 (1989).
[52] A. Juhin, F. De Groot, G. Vankó, M. Calandra, and C. Brouder, Angular dependence of core hole screening in $LiCoO_2$: A DFT + U calculation of the oxygen and cobalt K-edge x-ray absorption spectra, Phys. Rev. B **81**, 115115 (2010).
[53] I. Tanaka, T. Mizoguchi, and T. Yamamoto, Xanes and elnes in ceramic science, J. Am. Ceram. Soc. **88**, 2013 (2005).
[54] V. Kanchana, G. Vaitheeswaran, and M. Alouani, Calculated electronic structure and x-ray magnetic circular dichroism of CrO_2, J. Phys. Condens. Matter **18**, 5155 (2006).
[55] P. W. Anderson, Infrared Catastrophe in Fermi Gases with Local Scattering Potentials, Phys. Rev. Lett. **18**, 1049 (1967).
[56] E. A. Stern and J. J. Rehr, Many-body aspects of the near-edge structure in x-ray absorption, Phys. Rev. B **27**, 3351 (1983).
[57] K. Ohtaka and Y. Tanabe, Theory of the soft-x-ray edge problem in simple metals: Historical survey and recent developments, Rev. Mod. Phys. **62**, 929 (1990).
[58] M. S. Hybertsen and S. G. Louie, Electron correlation in semiconductors and insulators: Band gaps and quasiparticle energies, Phys. Rev. B **34**, 5390 (1986).